Journal of Materials Chemistry C

ROYAL SOCIETY OF CHEMISTRY

PAPER

View Article Online
View Journal

Cite this: DOI: 10.1039/d6tc00224b

Modulating electrochromic properties *via* thiophene donors in thieno[3,4-*c*]pyrrole-4,6-dione-based conjugated polymers

Kok Chan Chong, [abc] Kang Le Osmund Chin, [ab] Shi Jun Ang, [d] Ran Tao, [ab] Jianwei Xu *[a] and Ming Hui Chua *[ab]

Thieno[3,4-*c*]pyrrole-4,6-dione (TPD) is a strong imide-based electron acceptor that remains under-explored for electrochromic (EC) conjugated polymers, with existing studies limited by narrow donor scope and the use of varying device structures, hindering systematic structure–property comparisons. Herein, a series of seven TPD-based donor–acceptor conjugated polymers incorporating thiophene-derived donors, terthiophene, quaterthiophene, pentathiophene, thieno[3,2-*b*]thiophene (TT), 3,4-ethylenedioxythiophene (EDOT), dithieno[3,2-*b*:2′,3′-*d*]pyrrole (DTP), and cyclopenta[1,2-*b*:5,4-*b*′]dithiophene (CPDT), are synthesised to elucidate the roles of conjugation length, backbone planarity, and donor strength in governing EC properties. Systematic modulation of donor structures enables tuning of neutral-state colours from grey to purple and dark blue, while oxidised states exhibit different grey hues. Stronger electron-donating units significantly enhance EC performance, with the EDOT-based polymer exhibiting the highest optical contrasts of 23.8% (595 nm) and 46.7% (1800 nm), while the DTP-based polymer shows the best open circuit memory retention (*ca.* 74% retention of initial transmittance after 10 minutes), fastest response times of 4.3 (bleaching at 608 nm) and 6.8 s (colouration at 1400 nm) and highest coloration efficiencies of 801.1 and 1358.5 cm^2 C^{-1}. Meanwhile, long-term switching stability appears to be more influenced by polymer molecular weight, with the pentathiophene-based polymer having the highest weight average molecular weight (M_w) of 104.5 kDa, demonstrating the highest durability, retaining 79.1% of its initial optical contrast after 3000 cycles. In addition, the electrofluorochromic (EFC) behaviour is observed for five polymers, with the terthiophene-based polymer showing the best contrasts of $I_{OFF/ON}$ 11.7 for fluorescence switching at 710 nm. Overall, this work establishes a comprehensive structure–property framework for TPD-based EC polymers, providing design rules that enable predictive tuning of colour, efficiency, and stability, and supporting the rational and potentially data-driven development of future high-performance EC materials.

Received 22nd January 2026,
Accepted 13th April 2026

DOI: 10.1039/d6tc00224b

rsc.li/materials-c

1. Introduction

The colour switching properties of electrochromic (EC) materials under the control of external applied voltages make them highly useful and sought after for various applications such as smart windows, anti-glare vehicle rear mirrors, smart eyewear, optical displays, and even military camouflage.[1–5] Driven by increasing needs from energy-saving green buildings and automotive applications, the growing demand for EC materials and technologies can also be reflected by intensifying research in this area. Unlike traditional metal oxide-based EC materials, conjugated polymers offer unique advantages, such as colour tunability, light weight, flexibility, and solution processability at scale.[6] This proves to be especially useful for smart windows, the biggest driver for EC market growth, where the tints and colours of window panels in buildings and vehicles, as well as the extent of light and heat passing through, can be customized to the preferences and needs of homeowners, consumers, manufacturers, and developers.

Donor–acceptor (D–A) type conjugated polymers are widely studied for EC applications. They often exhibit robust EC

[a] *Institute of Sustainability for Chemicals, Energy and Environment (ISCE²), Agency for Science, Technology and Research (A*STAR), Singapore. 1 Pesek Road, Jurong Island, Singapore 627833, Republic of Singapore. E-mail: xu_jianwei@a-star.edu.sg, chua_ming_hui@a-star.edu.sg*
[b] *Institute of Materials Research and Engineering (IMRE), Agency for Science, Technology and Research (A*STAR), Singapore. 2 Fusionopolis Way, Innovis, #08-03, Singapore 138634, Republic of Singapore*
[c] *Future Energy Acceleration & Translation (FEAT), Strategic Research & Translational Thrust (SRTT), A*STAR Research Entities, 1 Fusionopolis Way, #20-10, Connexis North Tower, Singapore 138632, Republic of Singapore*
[d] *Institute of High Performance Computing (IHPC), Agency for Science, Technology and Research (A*STAR), Singapore. 1 Fusionopolis Way, #16-16, Connexis North Tower, Singapore 138632, Republic of Singapore*

switching performance, and offer tuneable optical properties such as EC switching colours *via* the rational selection of different aromatic electron-donor and electron-acceptor monomers. Common donors include thiophene-based monomers, triphenylamines, carbazoles, and pyrroles,[7–12] while common acceptors include quinoxalines, benzothiadiazoles (BTD), and triazoles.[13] Based on their different structures, and electron donating and withdrawing strengths, the selection and combination of monomers influence the polymers' frontier molecular orbital energies, absorption profiles, as well as optical and electronic bandgaps,[14–17] which may also have an effect on EC switching parameters, such as optical contrasts (OC), response times (τ), open circuit memory retention, colouration efficiencies (CE) and long-term switching stabilities. Based on this principle, numerous D–A type EC polymers bearing different acceptor groups have been developed over the years,[13] with reported working colours spanning almost the entire colour palette.[18,19] However, gaps still remain in the pursuit of precise colour tuning with the optimization of EC switching performance in the design of D–A type EC polymers. Future EC materials are expected to be increasingly tailored to application-specific requirements, guided by both expert intuition and emerging artificial intelligence and machine learning approaches.[20,21] In this context, a comprehensive understanding of structure–property relationships, particularly across a broader range of monomer building blocks, is essential to enable predictive control over EC switching colours and performance to rationally guide materials development.

Imide and amide-based acceptors are widely used building blocks for low-bandgap conjugated polymers with efficient charge transport in optoelectronic applications, owing to their strong electron-withdrawing characteristics and versatile functionalisation, for example through the introduction of different side chains at the nitrogen positions to fine-tune polymer properties.[22–25] Extensive studies have been carried out on EC polymers bearing diketopyrrolopyrrole,[26–29] isoindigo,[30–33] and rylene diimide[34–36] acceptors. Our team has also studied EC conjugated polymers with bay-isoindigo,[37] and pyromellitic diimide acceptors,[38] as well as polymers featuring novel diimide-based acceptors prepared *via* inverse electron-demand Diels Alder or Diels Alder reactions between different diimide precursors and triazine or tetrazine.[39–42] Polythiophenes are widely regarded as benchmark conjugated polymers due to their favourable photophysical and electronic properties for optoelectronic applications. Incorporation of thieno[3,4-*c*]pyrrole-4,6-dione (TPD) as an acceptor co-monomer provides an effective strategy to further tune these properties while largely preserving the planarity and rigidity of the polythiophene backbone. Conjugated polymers bearing a TPD acceptor have commonly been reported for photovoltaics[43–45] and field effect transistor applications,[46–49] and more recently, thermoelectrics[50] and photocatalysis.[51,52] Studies of TPD-based EC polymers are however limited, with only recent reports from Onal *et al.*,[53] Song *et al.*,[54] and Zhen *et al.*,[55] confined to bearing one to two thiophene, 3,4-ethylenedioxythiophene (EDOT), or 3,4-propylene dioxythiophene (ProDOT) donors (Table S3, SI). More importantly, with the limited choice of donors and varying EC device (ECD) structures used in these reports, it may be difficult to get a clear picture of important structure–property relationships of TPD-based EC polymers, which is crucial to guide future materials development.

To fully realise the potential of TPD as a versatile building block for high-performance EC polymers with tuneable colour, comprehensive structure–property relationship studies are required. In this study, seven TPD-based conjugated polymers bearing different numbers and types of thiophene(-based) donors (Scheme 1), p(TPD2T-T), p(TPD2T-2T), p(TPD2T-3T), p(TPD2T-TT), p(TPD2T-EDOT), p(TPD2T-DTP), and p(TPD2T-CPDT), were synthesized and studied for their EC properties. The use of different donors actually leads to a significant variation in neutral state colours from brown to magenta, purple and dark blue, while the oxidised state colours reveal different hues of grey. EC switching studies reveal that all polymers exhibit comparable OCs at both visible and near-infrared (NIR) wavelengths, while differing markedly in τ_s, CEs, and open-circuit memory. Polymers p(TPD2T-EDOT) and p(TPD2T-DTP), respectively incorporating stronger donors 3,4-ethylenedioxythiophene

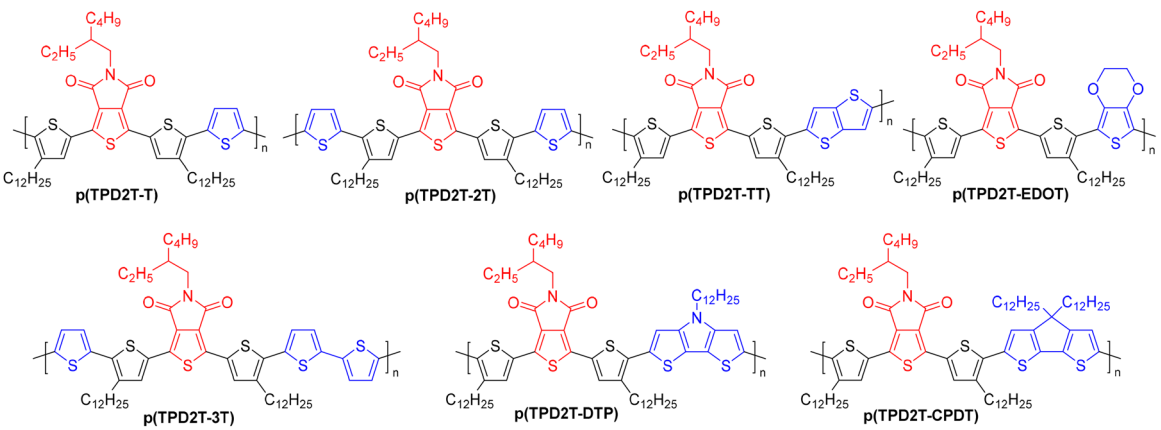

Scheme 1 Chemical structures of TPD-based EC polymers p(TPD2T-T), p(TPD2T-2T), p(TPD2T-3T), p(TPD2T-TT), p(TPD2T-EDOT), p(TPD2T-DTP), and p(TPD2T-CPDT) studied in this work.

(EDOT) and dithieno[3,2-*b*:2′,3′-*d*]pyrrole (DTP),[56] deliver superior performance: p(TPD2T-EDOT) exhibits the largest OC of 46.7% at 1800 nm, while p(TPD2T-DTP) shows the fastest switching τ_s (4.3/0.7 s for colouration/bleaching at 608 nm), the highest CE (1358.5 cm^2 C^{-1} at 1400 nm), and best open-circuit memory (retaining *ca.* 74% of its initial transmittance after 10 min). In contrast, p(TPD2T-3T), which has the highest weight-average molecular weight (M_w = 104.5 kDa), demonstrates the best long-term switching stability, retaining 79.1% of its initial OC after 3000 cycles. This polymer also exhibits the highest electrofluorochromic (EFC) switching contrast ($I_{OFF/ON}$ = 11.7 at 710 nm). Collectively, these results provide a comprehensive understanding of structure–property relationships in TPD-based EC polymers, addressing the current lack of systematic studies in this area.

2. Experimental

2.1. Materials and instruments

All chemical reagents and solvents used in the synthesis and purification of intermediates, monomers, and polymers, as well as in device fabrication, were purchased from commercial sources (Merck Sigma Aldrich; TCI; BLD Pharmatech; Tedia) and used without further purification unless otherwise stated. The purification of intermediates and monomers was performed *via* column chromatography using high purity grade silica gel (pore size 60 Å, mesh particle size 230–400, and particle size 40–63 μm) purchased from Merck Sigma Aldrich. NMR analysis was performed in deuterated solvents purchased from Cambridge Isotopes with tetramethylsilane (TMS) as the internal standard. ECDs use indium–titanium oxide (ITO)-coated glass substrates (15 Ω sq^{-1}; 30 × 35 × 1.1 mm) purchased from Xin Yan Technology Ltd.

^1H and ^{13}C NMR spectra were recorded in deuterated solvents using a Bruker AV400SB 400 MHz NMR spectrometer, with chemical shifts expressed in parts per million (ppm) relative to the TMS reference. High resolution electron spray ionization mass spectrometry (ESI) was performed using an Agilent LC-QTOF 6545B. Gel permeation chromatography (GPC) was performed in THF solutions using an Agilent 1260 Infinity II GPC/SEC system using polystyrene as the standard. UV-Vis-NIR absorption spectra of polymer solutions, and EC spectroelectrochemistry together with kinetic switching studies were recorded and performed using an Agilent Cary 5000 UV-Vis-NIR spectrophotometer. A PalmSens4 Potentiostat/Galvanostat was used to perform cyclic voltammetry (CV) and apply voltages for EC spectroelectrochemistry and kinetic switching studies. CV studies were performed in a three-electrode cell configuration with a glassy carbon working electrode, a Pt wire counter electrode and an Ag wire pseudo-reference electrode. Polymers were dissolved in 0.1 M $TBAPF_6$ DCM solution for solution CV studies, whereas polymers were deposited over a glassy carbon working electrode and immersed into 0.1 M $LiClO_4$ in acetonitrile electrolyte for thin-film CV studies. CV studies were performed at a scan rate of 50 mV s^{-1}, and referenced against the ferrocene/ferrocenium (Fc/Fc^+) redox couple. Fourier-transform infrared (FTIR) spectra of polymers were recorded using a Bruker Vertex 70 FTIR spectrometer. Colorimetric analysis was performed using a Hunterlab ColorQuest XE colorimeter. Thermal gravimetric analysis (TGA) and differential scanning calorimetry (DSC) were performed on a TA Instruments TGA Q500 and PDSC Q100, respectively. The thickness of spin-coated polymer films on ITO/glass substrates were measured *via* surface profilometry using a KLA Tencor P16 surface profiler. Scanning electron microscopy (SEM) was performed using a Hitachi SU8220 field emission SEM.

2.2. Device fabrication

Sandwiched-type thin film ECDs were fabricated with the following device configuration: glass|ITO|EC polymer|gel electrolyte|ITO|glass. ITO–glass substrates were first cleaned with deionized water and acetone under ultrasonication, followed by ozone surface treatment at 100 °C for 10 minutes. 150 μL of polymer solution (10 mg mL^{-1} in chloroform/chlorobenzene 1 : 1 v/v, filtered over 0.45 μm PVDF filter frit) was pipetted onto the ITO surface of one pre-cleaned substrate and spin-coated at 500 rpm for 30 s using a Laurell WS-400-LITE spin-coater. The substrate was allowed to stand on a hotplate at 80 °C for a minute. The excess edges on the spin-coated substrates were wiped off with a cotton bud to obtain a 2 × 2 cm active area. Meanwhile, 250 μL of gel electrolyte, prepared by stirring 0.512 g $LiClO_4$, 6.65 mL of propylene carbonate, and 2.8 g of PMMA (M_w 120k g mol^{-1}), was pipetted onto the ITO surface of another substrate over a 2 × 2 cm demarcated area blocked-out by double-sided tape, and allowed to stand for 15–20 minutes. The ECDs were then assembled by sandwiching the two substrates with 0.5 cm of uncontacted edges on each substrate for electrical contact.

2.3. EC switching studies

Spectroelectrochemistry studies were performed by measuring the absorption spectra of ECDs with different voltages applied from the potentiostat connected *via* crocodile clips and wiring. Likewise, for kinetic switching/chronoabsorptometry studies, the transmittances of ECDs at selected wavelengths were monitored over time as the voltage applied was varied. The optical contrasts (OCs) are measured in terms of maximum change in transmittance under a constant applied voltage, whereas the switching speed or response times (τ) was determined by the time taken for the ECD to achieve 95% maximum OC in either the oxidative or subsequent reductive recovery colouration process. Colouration efficiency (CE) is defined as the change in optical density per unit charge input or removed. It is determined with the formula $CE = \log(T_{ox}/T_{red})/(q/A)$, where T_{ox} and T_{red} are the absolute transmittance of the ECDs measured in the oxidised and reduced states, respectively, q is the charge input or removed, and A is the active area (2 × 2 cm = 4 cm^2). Open circuit memory was determined by monitoring the transmittance over time upon removing electrical contact. Finally, long-term switching stability was likewise studied by monitoring the transmittance over time as applied

voltage alternates between a positive and negative voltage with a pre-determined time interval over up to 1000 cycles.

2.4. Synthesis and characterization

The synthesis of the seven polymers is outlined in Scheme S1, SI.

1,3-Bis(4-dodecylthiophen-2-yl)-5-(2-ethylhexyl)-4*H*-thieno-[3,4-*c*]pyrrole-4,6(5*H*)-dione (2). 1,3-Bis(5-bromothiophen-2-yl)-5-(2-ethylhexyl)-4*H*-thieno[3,4-*c*]pyrrole-4,6(5*H*)-dione (212 mg, 0.50 mmol), (4-dodecylthiophen-2-yl)trimethylstannane (519 mg, 1.25 mmol), and $Pd(PPh_3)_2Cl_2$ catalyst (18 mg, 0.025 mmol) were added into a flame-dried Schlenk flask and the reaction chamber was evacuated and backfilled with argon gas 3 times. Anhydrous tetrahydrofuran (10 mL) was added *via* a needle and syringe, and the reaction mixture was stirred at 80 °C for 18 hours. Upon cooling to room temperature, water was added, and the mixture was extracted with dichloromethane 3 times. The combined organic layer was dried over anhydrous magnesium sulphate, filtered and concentrated. Column chromatography with a dichloromethane/hexane (1 : 4 v/v) eluent was performed to isolate the product as a yellow solid (332 mg, 87% yield). ^{1}H NMR (500 MHz, $CDCl_3$, δ): 0.88–0.94 (m, 12H), 1.32–1.44 (m + s, 40H), 1.90 (t, J = 5.8 Hz, 2H), 3.64–3.75 (m, 4H), 7.16 (s, 2H), 7.47 (dd, J = 8.0 Hz, 0.8 Hz, 2H), 9.12 (d, J = 8.0 Hz, 2H). ^{13}C NMR (100 MHz, $CDCl_3$, δ): 10.7, 14.1, 23.03, 24.1, 24.9, 28.6, 30.5, 37.4, 44.1, 83.5, 84.0, 113.3, 113.6, 124.2, 128.7, 128.9, 134.3, 144.4, 168.1. HRMS (ESI, m/z): $[M + H]^+$ calculated for $C_{44}H_{65}B_2N_2O_6$, 739.5023; measured, 739.5026.

1,3-Bis(5-bromo-4-dodecylthiophen-2-yl)-5-(2-ethylhexyl)-4*H*-thieno[3,4-*c*]pyrrole-4,6(5*H*)-dione (3). A flame-dried Schlenk flask was charged with compound **2** (306 mg, 0.4 mmol) and the *N*-bromosuccinimide (171 mg, 0.96 mmol), which was then evacuated and backfilled with argon gas 3 times. Chloroform (3 mL) and acetic acid (3 mL) were then added, and the reaction mixture was allowed to stir at room temperature for 16 hours. Afterwards, water was added, and the mixture was extracted with dichloromethane (DCM) 3 times. The combined organic layer was dried over anhydrous magnesium sulphate, filtered and concentrated. Column chromatography with a dichloromethane/hexane (1 : 4 v/v) eluent was performed to isolate the product as a yellow solid (314 mg, 85% yield). ^{1}H NMR (500 MHz, $CDCl_3$, δ): 0.84–0.88 (m, 12 H), 1.23–1.34 (m, 64 H), 1.92 (m, J = 2H), 3.69 (d, J = 7.3 Hz, 4H), 4.27 (m, 4H), 4.34 (m, 4H), 6.37 (s, 2H), 7.24 (d, J = 1.5 Hz, 2H), 7.33 (dd, J = 8.5 Hz, 2.7 Hz, 2H), 9.12 (d, J = 8.5 Hz, 2H). ^{13}C NMR (100 MHz, $CDCl_3$, δ): 14.1, 22.7, 26.7, 29.3, 29.6, 29.7, 30.0, 31.8, 31.9, 36.5, 44.4, 64.4, 64.9, 99.2, 105.3, 117.8, 119.0, 120.2, 129.7, 131.7, 136.6, 139.5, 142.4, 145.3, 168.8. HRMS (ESI, m/z): $[M]^+$ calculated for $C_{68}H_{98}N_2O_6S_2$, 1103.6939; measured, 1103.6935.

General procedure for Stille polymerization. To a flame-dried Schlenk flask connected to the Schlenk line, the dibromide and bis(trimethyltin) monomers were dissolved in anhydrous toluene under an inert gas atmosphere in a 1 : 1 molar equivalence ratio at a monomer concentration of 10 M. The $Pd(PPh_3)_4$ catalyst (0.05 equivalence) was added and the reaction mixture thoroughly degassed by the freeze–pump–thaw method. The reaction mixture was allowed to stir at 100 °C for 24 h, and thereafter upon cooling down to room temperature, the reaction mixture was added dropwise into a large excess of methanol to precipitate out the crude product. The crude product was collected *via* simple filtration, dried and purified using a Soxhlet extractor setup first by washing with hot methanol, acetone and hexane, and then extracted with chloroform. The solvent was removed using a rotary evaporator and the polymer product was washed with methanol, collected *via* simple filtration, and finally dried using a vacuum oven.

p(TPD2T-T) was synthesized *via* Stille polymerization between compound **3** and 2,5-bis(trimethylstannyl)thiophene to afford a shiny purple solid (98.0% yield). ^{1}H NMR (500 MHz, $CDCl_3$, δ): 0.85 (m, 12H), 1.11–1.59 (m, broad, 64H), 1.89 (broad, 2H), 3.74 (broad, 4H), 6.67 (broad, 2H), 7.05 (broad, 2H), 7.47 (broad, 2H), 9.04 (broad, 2H). GPC using PS in THF as a standard (M_n = 9017, M_w = 9 350, PDI = 1.037). FTIR (KBr): ν (cm^{-1}) = 2918 (s), 2849 (s), 1690 (m), 1607 (s), 1457 (m), 1112 (m), 790 (m).

p(TPD2T-2T) was synthesized *via* Stille polymerization between compound **3** and 5,5′-bis(trimethylstannyl)-2,2′-bithiophene to afford a shiny purple solid (93.0% yield). ^{1}H NMR (500 MHz, $CDCl_3$, δ): 0.86 (broad, 12H), 1.25 (broad, 64 H), 3.73 (broad, 4H), 6.06–6.66 (m, broad, 8H), 8.62 (m, broad, 2H). GPC using PS in THF as a standard (M_n = 12 145, M_w = 17 822, PDI = 1.467). FTIR (KBr): ν (cm^{-1}) = 2921 (s), 2851 (s), 1687 (s), 1607 (s), 1453 (m), 1358 (m), 1111 (m), 786 (m).

p(TPD2T-3T) was synthesized *via* Stille polymerization between compound **3** and 5,5′′-bis(trimethylstannyl)-2,2′:5′,2′′-terthiophene to afford a shiny purple solid (14.0% yield). ^{1}H NMR (500 MHz, $CDCl_3$, δ): 0.86 (s, broad, 12H), 1.25 (broad, 64 H), 1.84 (broad, 2H), 3.67 (broad, 4H), 6.89 (m, broad, 6H), 7.56 (m, broad, 4H), 9.01 (m, broad, 2H). GPC using PS in THF as a standard (M_n = 54 295, M_w = 104 517, PDI = 1.925). FTIR (KBr): ν (cm^{-1}) = 2921 (s), 2850 (s), 1687 (m), 1607 (s), 1456 (m), 1111 (m), 783 (m).

p(TPD2T-TT) was synthesized *via* Stille polymerization between compound **3** and 2,5-bis(trimethylstannyl)thieno[3,2-*b*]thiophene to afford a shiny purple solid (99.0% yield). ^{1}H NMR (500 MHz, $CDCl_3$, δ): 0.84–0.88 (m, broad, 12H), 1.25 (broad, 64H), 4.02 (broad, 4H), 6.42 (broad, 4H), 7.47 (broad, 2H), 8.70 (broad, 2H). GPC using PS in THF as a standard (M_n = 13 546, M_w = 21 500, PDI = 1.587). FTIR (KBr): ν (cm^{-1}) = 2921 (s), 2852 (m), 1687 (m), 1607 (s), 1459 (m), 1112 (s), 801 (m).

p(TPD2T-EDOT) was synthesized *via* Stille polymerization between compound **3** and 5,7-bis(trimethylstannyl)-2,3-dihydrothieno[3,4-*b*][1,4]dioxine to afford a shiny blue solid (70.4% yield). ^{1}H NMR (500 MHz, $CDCl_3$, δ): 0.93–0.99 (broad, 12H), 1.37 (broad, 16H), 1.84 (broad, 2H), 3.70 (broad, 4H), 4.44 (broad, 4H), 7.05–7.17 (m, broad, 2H), 7.47 (m, broad, 2H), 9.03–9.09 (m, broad, 2H). GPC using PS in THF as a standard (M_n = 5 078, M_w = 9650, PDI = 1.784). FTIR (KBr): ν (cm^{-1}) = 2919 (m), 2854 (m), 1687 (s), 1604 (s), 1431 (s), 1351 (s), 1105 (s), 872 (m).

p(TPD2T-DTP) was synthesized *via* Stille polymerization of compound **3** and 4-dodecyl-2,6-bis(trimethyltin)-4*H*-dithieno-[3,2-*b*:2′,3′-*d*]pyrrole to afford a shiny blue solid (90.0% yield). ^{1}H NMR (500 MHz, $CDCl_3$, δ): 0.86 (m, broad, 12H), 1.26 (m, broad, 64 H), 1.92 (broad, 2H), 3.70 (broad, 4H), 4.35–4.43

(m, 8H), 7.34 (m, broad, 2H), 7.47 (m, broad, 2H), 9.12 (broad, 2H). GPC using PS in THF as a standard (M_n = 6300, M_w = 10 632, PDI = 1.688). FTIR (KBr): ν (cm^{-1}) = 2921 (s), 2851 (s), 1687 (m), 1607 (s), 1450 (s), 1358 (s), 1114 (s), 1082 (s).

p(TPD2T-CPDT) was synthesized *via* Stille polymerization between compound **3** and 2,6-bis(trimethyltin)-4,4-bis(2-dodecylbenzo)-4*H*-cyclopenta[2,1-*b*:3,4-*b*′]dithiophene to afford a shiny purple solid (90.0% yield). ^{1}H NMR (500 MHz, $CDCl_3$, δ): 0.86 (m, broad, 12H), 1.26 (m, broad, 64 H), 1.92 (broad, 2H), 3.70 (broad, 4H), 4.35–4.43 (m, 8H), 7.34 (m, broad, 2H), 7.47 (m, broad, 2H), 9.12 (broad, 2H). GPC using PS in THF as a standard (M_n = 10 496, M_w = 19 442, PDI = 1.852). FTIR (KBr): ν (cm^{-1}) = 2921 (s), 2851 (s), 1687 (m), 1607 (s), 1450 (s), 1358 (s), 1114 (s), 1082 (s).

3. Results and discussion

3.1. Polymer synthesis and characterization

The polymers p(TPD2T-T), p(TPD2T-2T), p(TPD2T-3T), p(TPD2T-TT), p(TPD2T-EDOT), p(TPD2T-DTP), and p(TPD2T-CPDT) were synthesized by co-polymerizing bis(5-bromo-4-dodecylthiophen-2-yl)-TPD monomer with the di-stannylated monomers of thiophene (T), bithiophene (2T), terthiophene (3T), thieno[3,2-*b*]thiophene (TT), EDOT, *N*-dodecyl DTP, and 4,4-didodecyl cyclopenta[1,2-*b*:5,4-*b*′]dithiophene (CPDT), respectively, *via* Stille cross-coupling polymerization and then purified by Soxhlet extraction (Scheme S1, SI). The choice of these seven thiophene-based co-monomers represent distinct structural classes, including linear oligothiophenes with increasing conjugation length (T, 2T, 3T), fused thiophene systems with enhanced planarity (TT, CPDT), and stronger donor characteristics (EDOT, DTP), thus enabling a systematic evaluation of structure–property relationships in TPD-based EC polymers. All seven polymers were relatively soluble in chlorinated solvents, hence rendering them solution processable. The conscious efforts to introduce long dodecyl chains helps to improve polymer solubility. The polymers were synthesized in good yields of >70%, except for p(TPD2T-3T) due to relatively low solubility, given its low alkyl-to-aromatic groups ratio, hence lesser polymers extracted by hot chloroform. The polymers exhibit comparable weight average molecular weights (M_w) between 9.4 and 21.5 kDa, except for p(TPD2T-3T) which has an exceptionally large M_w of 104.5 kDa. All seven polymers exhibit a good poly-dispersity index (PDI) of 1.04 to 1.93 (Table S1, SI).

Due to the rigid, π-conjugated backbones and associated intermolecular aggregation, ^{1}H NMR spectra of the seven polymers measured in both $CDCl_3$ and toluene-d^6 exhibit broadened signals characteristic of reduced chain mobility. In the aromatic region ($\delta \sim$ 6.5–8.5 ppm), broad low-intensity resonances are assigned to protons of the thiophene/thiophene-based donors. In the downfield aliphatic region ($\delta \sim$ 2.5–4.0 ppm), weak, broadened low-intensity signals correspond to the methine and methylene protons adjacent to the branching point of the 2-ethylhexyl substituent on the TPD unit, as well as the α- and β-methylene protons of alkyl chains/groups attached to electron-rich thiophene/thiophene-based donor units (*e.g.*, EDOT and DTP). The upfield region ($\delta \sim$ 0.5–2.0 ppm) is dominated by intense, broad resonances arising from the remaining methylene and terminal methyl protons of the dodecyl and 2-ethylhexyl side chains. FTIR spectra of all seven polymers consistently exhibit strong bands at ~1670 and 1738 cm^{-1}, attributed to the C=O stretching vibrations of the TPD acceptor units. Intense bands in the range of ~2850–2960 cm^{-1} correspond to the aliphatic C–H stretching vibrations of the 2-ethylhexyl and dodecyl side chains. Additionally, weak bands at ~3065–3070 cm^{-1} are observed and assigned to aromatic C–H stretching of the thiophene-based units. Thermogravimetric analysis (TGA) of the seven polymers also shows that the polymers show considerable thermal stability with decomposition temperatures (at which 5% weight loss occurs) between 230.68 and 415.13 °C.

3.2. Optical and electrochemical properties

Table 1 summarises the optical and electrochemical properties of the seven TPD polymers. Fig. 1a shows the normalized absorption spectra of the TPD polymers in chloroform solutions. All seven polymers exhibit a main absorption band across the visible region with a shoulder peak observed at 658 and 624 nm for p(TPD2T-TT) and p(TPD2T-T), respectively. Increasing the number of thiophene donors per repeating unit from three in p(TPD2T-T) to four and five in p(TPD2T-2T) and p(TPD2T-3T) led to a slight blueshift in λ_{abs} from 510 nm to 494 and 498 nm, respectively,

Table 1 Summary of optical and electrochemical properties of the seven TPD polymers

Polymer	$\lambda_{abs}^{Soln\,a}$ (nm)	ε^b (M^{-1} cm^{-1})	$\lambda_{onset}^{Soln\,c}$ (nm)	$E_g^{Opt\,d}$ (eV)	$\lambda_{abs}^{Film\,e}$ (nm)	$\lambda_{PL}^{Soln\,f}$ (nm)	$\lambda_{PL}^{Film\,g}$ (nm)	$E_{Onset}^{Ox\,h}$ (V)	$E_{HOMO}{}^{i}$ (eV)	$E_{LUMO}{}^{j}$ (eV)
p(TPD2T-T)	510, 624 (sh)	30 818	700	1.77	492	604	710	0.97	−5.77	−4.00
p(TPD2T-2T)	494	35 219	693	1.79	490	608	708	0.79	−5.59	−3.80
p(TPD2T-3T)	498	40 118	697	1.78	520	602	697	0.55	−5.35	−3.57
p(TPD2T-TT)	520, 658 (sh)	30 413	693	1.79	497	610	710	0.85	−5.65	−3.86
p(TPD2T-EDOT)	537	22 159	747	1.66	595	625	—	0.59	−5.39	−3.73
p(TPD2T-DTP)	565	34 218	780	1.59	608	655	—	0.42	−5.22	−3.63
p(TPD2T-CPDT)	558	36 289	685	1.81	555	666	715	0.52	−5.32	−3.51

[a] Absorption maximum wavelength in chloroform solution. [b] Molar extinction coefficient. [c] Absorption onset wavelength. [d] Optical bandgap = $1240/\lambda_{onset}^{Soln}$. [e] Absorption maximum wavelength of the thin film. [f] Photoluminescence maximum wavelength in chloroform solution. [g] Photoluminescence maximum wavelength of the thin film. [h] Oxidation onset potential determined by solution CV, *vs.* Fc/Fc^+. [i] HOMO energy level = E_{Onset}^{Ox} − (−4.8) eV. [j] LUMO energy level = $E_{HOMO} + E_g^{Opt}$.

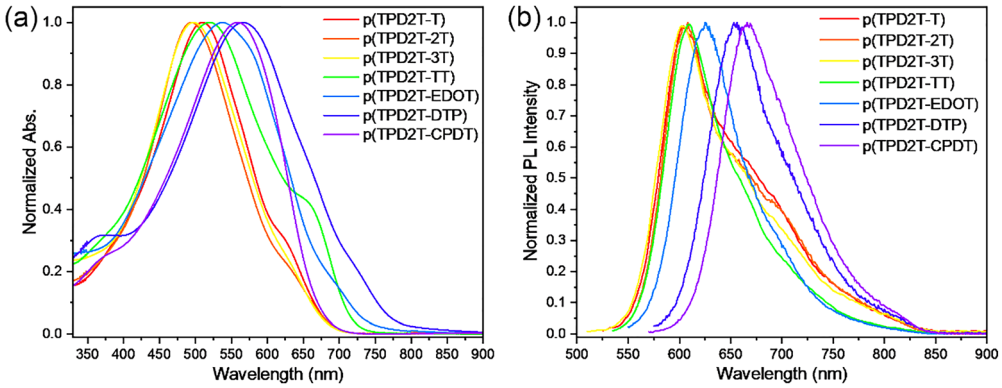

Fig. 1 Normalized absorption (a) and photoluminescence (b) spectra of polymers p(TPD2T-T), p(TPD2T-2T), p(TPD2T-3T), p(TPD2T-TT), p(TPD2T-EDOT), p(TPD2T-DTP), and p(TPD2T-CPDT) in chloroform solution.

together with steady increase in molar absorption coefficient (ε) from 30 818 to 35 219 and 40 118 M^{-1} cm^{-1}. The largest ε registered for p(TPD2T-3T) amongst the seven polymers could also be due to its exceptionally high M_w. Meanwhile, replacing a thiophene in each repeating unit of p(TPD2T-T) with thiophene-based donors thieno[3,2-*b*]thiophene (TT), EDOT, DTP, and cyclopenta[1,2-*b*:5,4-*b*′]dithiophene (CPDT), led to significant red-shift in λ_{abs} for p(TPD2T-TT), p(TPD2T-EDOT), p(TPD2T-DTP), and p(TPD2T-CPDT), at 520, 537, 565, and 558 nm, respectively. p(TPD2T-DTP) exhibits the most red-shifted absorption profile, which can be attributed to the strong electron-donating characteristic of the DTP unit and its ability to enhance intramolecular charge transfer (ICT) with the TPD acceptor, thereby reducing the bandgap. λ_{abs} of polymers p(TPD2T-T), p(TPD2T-2T), p(TPD2T-TT), and p(TPD2T-CPDT) in thin films were either comparable or slightly blue-shifted compared to that in solutions, whereas the thin film λ_{abs} of polymers p(TPD2T-3T), p(TPD2T-EDOT) and p(TPD2T-DTP) showed obvious red-shifting (Table 1 and Fig. 3).

Based on the absorption spectra onsets, the seven TPD polymers were determined to have rather low optical bandgaps (E_g) between 1.66 and 1.81 eV. Increasing the number of thiophene per repeating unit from 3 to 4 and 5, as well as the introduction of the TT donor did not result in remarkable differences in E_g amongst p(TPD2T-T), p(TPD2T-2T), p(TPD2T-3T) and p(TPD2T-TT), respectively. As compared to p(TPD2T-T), the introduction of stronger EDOT and DTP donors led to marked reduction in E_g for p(TPD2T-EDOT) and p(TPD2T-DTP) (1.77 *vs.* 1.66 *vs.* 1.59 eV, respectively). Meanwhile, with the CPDT donor, the E_g of p(TPD2T-CPDT) was slightly increased to 1.81 eV. The HOMO energy levels (E_{HOMO}) of the polymers, as determined by cyclic voltammetry (Fig. S1, SI), were found to be correlate well with the strength of the thiophene-based donors, with polymer p(TPD2T-DTP) having the highest E_{HOMO} of −5.22 eV and the lowest oxidation potential of 0.42 eV. This is consistent with DTP being the most electron-rich donor amongst those present in the seven polymers, which is often used to design low band-gap conjugated polymers exhibiting similar characteristics.[56] Meanwhile, the LUMO energy levels (E_{LUMO}) of the seven polymers were determined and found to be in the range between −3.51 and −4.00 eV (Table 1).

All seven polymers exhibit deep-red fluorescence in solutions, with photoluminescence (PL) maximum wavelengths (λ_{PL}) ranging between 604 and 666 nm (Fig. 1b). Polymers p(TPD2T-T), p(TPD2T-2T), p(TPD2T-3T), and p(TPD2T-TT) have fairly comparable fluorescence profiles whereas the introduction of EDOT, DTP, and CPDT donors markedly red-shifted the fluorescence spectra of p(TPD2T-EDOT), p(TPD2T-DTP), and p(TPD2T-CPDT), leading to λ_{PL} values of 625, 655, and 666 nm, respectively (*vs.* 604 nm for p(TPD2T-T)). Thin films of p(TPD2T-EDOT) and p(TPD2T-DTP) appear non-fluorescent, while the thin film fluorescence of the remaining polymers were red-shifted compared to that in the corresponding solutions (Fig. S3, SI). The red-shift in fluorescence could be attributed to stronger intermolecular π–π stacking between polymer chains in thin films, which causes greater structural planarity in the polymer backbones and enhances electron delocalization, thus effectively reducing emission energy.[57] As such, p(TPD2T-CPDT), which is structurally more rigid and planar in solution due to the CPDT donor, experiences only a small redshift in λ_{PL} of 49 nm in the thin film, while p(TPD2T-T) being less rigid and planar in solution, experiences only a greater redshift in λ_{PL} of 106 nm in the thin film.

3.3. Density functional theory (DFT) calculations

To further understand the effects of different thiophene-based donors on the optical properties of TPD polymers, we first performed conformational sampling of full monomeric units of the TPD polymers using the Global Optimization Algorithm (GOAT)[58] in conjunction with the GFN2-xTB semiempirical Hamiltonian[59] to obtain the lowest energy conformers. Implicit solvation was considered *via* the analytical linearized Poisson–Boltzmann (ALPB) model[60] with chloroform as solvent. Upon obtaining the lowest energy structures, all long aliphatic chains were replaced with a methyl group (Fig. 2), and the truncated structures were refined with DFT at the SMD(chloroform)-MN15/def2-SVP level of theory.[61,62] All dihedral angles were fixed during the DFT optimization. This retains the intramolecular influences of the respective long alkyl chains on

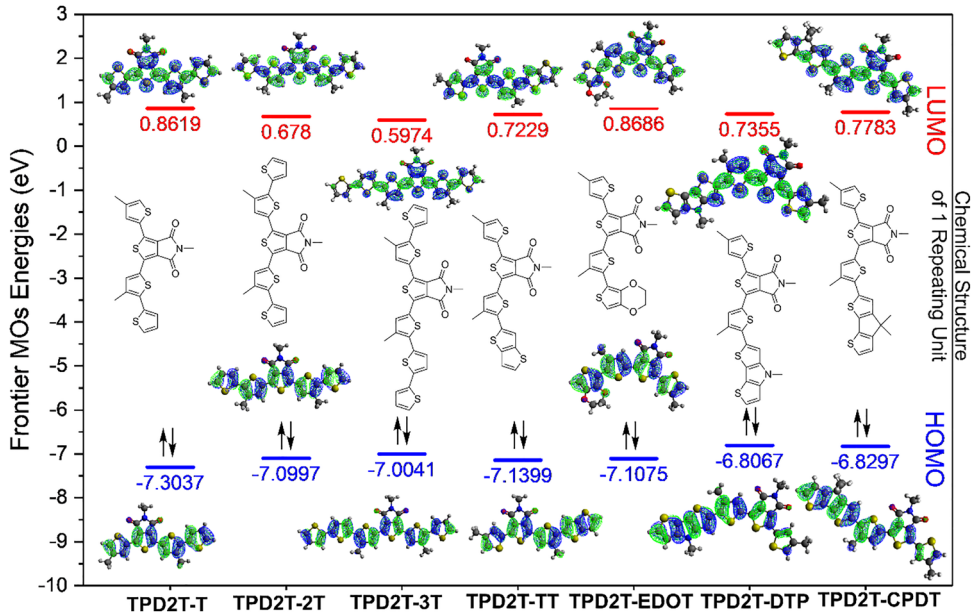

Fig. 2 DFT calculated HOMOs and LUMOs and their respective energies (MN15/def2-SVP) of one repeating unit of the TPD polymers (structures shown in the figure) studied in this work.

the conformations of the core structures, while having visual clarity on the characteristics of the frontier MOs. We believe that the truncation approach is appropriate due to the negligible contributions of the atomic orbitals, centred on the atoms of the alkyl chains, to the frontier MOs.

The DFT-calculated HOMOs and LUMOs of the seven structures display relatively uniform electron-density distributions along the oligo-thiophene backbones, indicative of delocalized π and π* frontier orbitals. This delocalization is expected to facilitate intrachain charge transport upon electrochemical doping, thus is beneficial for efficient EC switching in the corresponding polymers.[63] The calculated HOMO and LUMO energies for the repeating units agree with the trend of E_{HOMO} and E_{LUMO} of the seven polymers (Table 1). This includes modest reduction of the calculated HOMO–LUMO energy gaps from TPD2T-T to TPD2T-2T and TPD2T-3T. Meanwhile, replacing a thiophene unit with TT, slightly extending π-conjugation, resulted in a slightly higher HOMO and lower LUMO for TPD2T-TT relative to TPD2T-T. Substituting a thiophene unit with stronger EDOT, DTP, and CPDT donors gave higher HOMO energies in TPD2T-EDOT, TPD2T-DTP, and TPD2T-CPDT, with TPD2T-DTP having the highest calculated HOMO energy of −6.807 eV (*vs.* −7.304 eV of TPD2T-T). All computations were carried out with ORCA 6.1.1.[64]

3.4. EC spectroelectrochemistry

The polymers were soluble in chlorinated organic solvents, making them solution processable for opto-electronics device fabrication. Herein, thin film ECDs were fabricated to study the EC properties of the seven polymers, where they were spin-coated over ITO/glass substrates as part of the fabrication process. SEM under 1500× and 6000× magnifications show that the spin-coated polymer films generally possess homogenous morphologies (Fig. S4, SI). Polymers p(TPD2T-TT), p(TPD2T-EDOT), and p(TPD2T-DTP) form notably more homogeneous and smoother films with minimal phase separation, suggesting superior film-forming ability. In contrast, p(TPD2T-T), p(TPD2T-2T) and p(TPD2T-CPDT) films reveal rougher surface textures reflecting poorer film uniformity, with p(TPD2T-T) showing granular features under 6000× magnification, while p(TPD2T-2T) and p(TPD2T-CPDT) exhibit distinct island-like phase segregation features. The differences in film morphologies are expected to influence charge distribution during EC switching, thereby affecting device performance, to be discussed later.

While the absorption spectra of the seven polymers did not show noticeable changes on the application of increasing negative voltages, they exhibit gradual changes with increasing positive voltages, as shown in Fig. 3a–g, revealing the anodically-colouring nature of these TPD-based conjugated polymers. The respective changes in absorption spectra are due to the formation of polarons and bipolarons when the polymers undergo electro-oxidation. In the neutral state, the polymers show an intense absorption band with λ_{abs} between 490 and 612 nm in the visible region, and a low intensity and broad absorption band stretching into the NIR region, likely arising from strong intermolecular π–π interactions, excitonic coupling and charge-transfer states in the solid thin film state. Increasing applied voltages to a polymer generally led to the gradual collapse of its visible absorption band, accompanied by the emergence of a far-red absorption band and another broader NIR absorption band. For the polymers p(TPD2T-T), p(TPD2T-2T) and p(TPD2T-3T), changes in the absorption spectra occur from *ca.* +1.0 to +1.2 V. The incremental absorption changes for the three polymers appear to taper off at +2.2, +2.2, and +2.0 V, respectively. Beyond this point, distinctly new absorption profiles with λ_{abs} ranging from *ca.* 420 to 375 nm

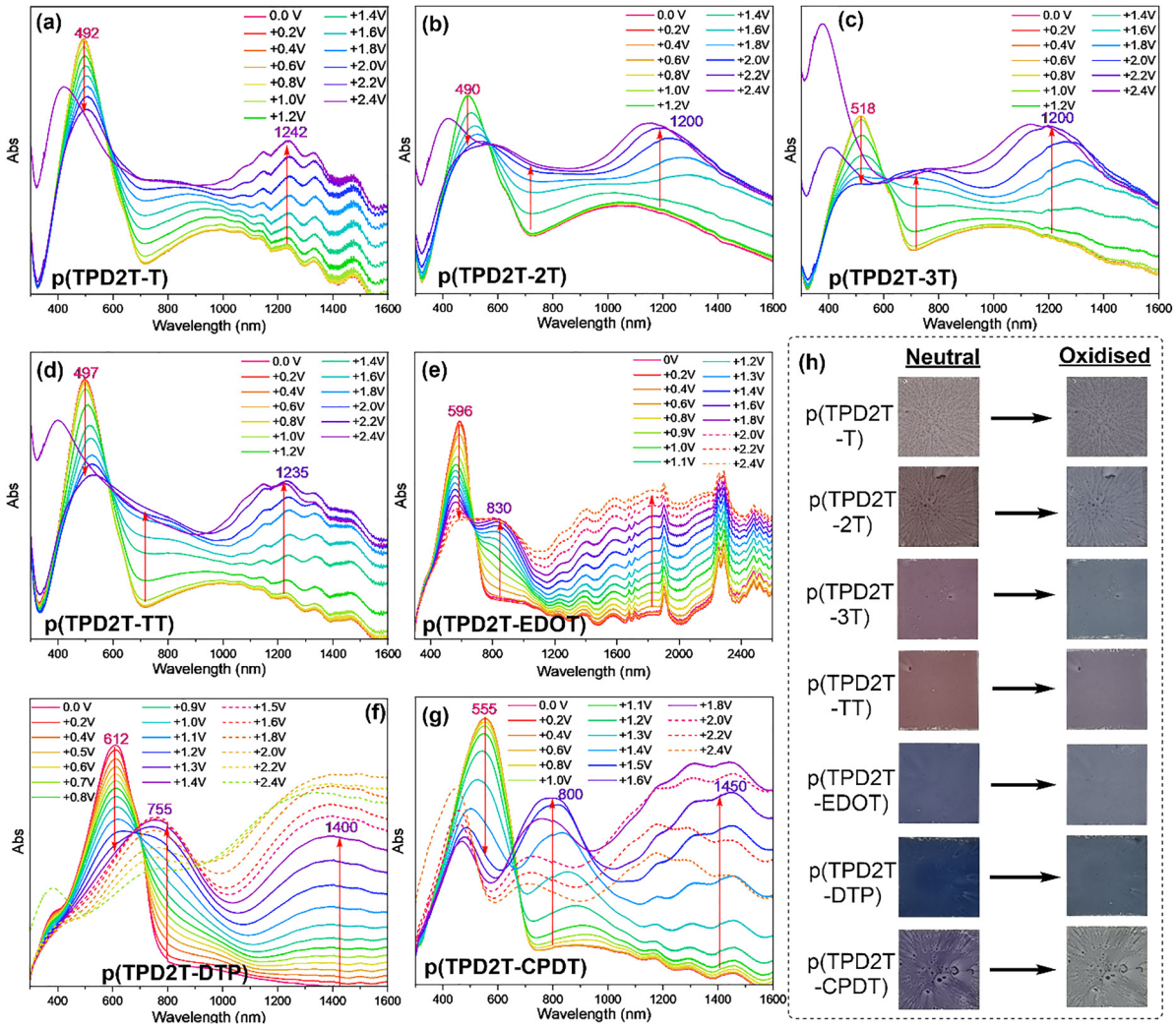

Fig. 3 EC spectroelectrochemistry of the (a) p(TPD2T-T), (b) p(TPD2T-2T), (c) p(TPD2T-3T), (d) p(TPD2T-TT), (e) p(TPD2T-EDOT), (f) p(TPD2T-DTP), and (g) p(TPD2T-CPDT) polymers with increasing applied voltages from 0.0 to +2.4 V. (h) EC colour changes of the seven polymers upon undergoing electro-oxidation.

emerge as applied voltages increase. Going from p(TPD2T-T) to p(TPD2T-2T) and p(TPD2T-3T), the intensities of newly-emerged NIR absorption bands increase relative to the absorbance in the visible regions (at 492, 490, and 518 nm, respectively) in the oxidised states (Fig. 3a–c). Likewise, the p(TPD2T-TT) polymer showed incremental spectral changes from +1.0 V until +2.2 V, where the absorption intensities at both 525 and 1235 are somewhat comparable (Fig. 3d).

Meanwhile, with the introduction of stronger donors, EDOT and DTP, the onset of absorption spectral changes for the p(TPD2T-EDOT) and p(TPD2T-DTP) polymers occurred much earlier at +0.4 and +0.2 V, respectively. The respective single neutral state absorption band at λ_{abs} of 596 and 612 nm gradually collapsed with increasing applied voltages, transitioning into a new far-red absorption band at λ_{abs} at 830 and 755 nm, respectively. This transition was accompanied by another broader new NIR absorption band at λ_{abs} of *ca.* 1825 and 1400 nm, respectively, with comparable intensities (Fig. 3e and f). This transition appears to taper off at *ca.* +1.5 V for p(TPD2T-DTP), after which the NIR absorbance at 1400 nm continues to rise until +2.0 V before dropping, while the far-red absorbance at 755 nm starts to reduce. For polymer p(TPD2T-CPDT), absorption spectra change occurs starting from +0.8 V. At +1.6 V, the electro-oxidised polymer shows three distinct absorption bands at λ_{abs} *ca.* 470, 800, and 1450 nm (Fig. 3g). Further increasing the applied voltages led to a decrease in the far-red and NIR absorbance, accompanied by an increase in the blue absorbance at *ca.* 450 nm.

In the neutral state, the polymers revealed a range of colours from light grey to brown, magenta brown, and reddish brown for p(TPD2T-T), p(TPD2T-2T), p(TPD2T-3T), and p(TPD2T-TT), respectively, as well as greyish blue, dark blue, and purple for polymers with stronger donors, p(TPD2T-EDOT), p(TPD2T-DTP), and p(TPD2T-CPDT), respectively. The corresponding colour changes for polymers p(TPD2T-T), p(TPD2T-2T), p(TPD2T-3T), p(TPD2T-TT), p(TPD2T-EDOT), p(TPD2T-DTP),

and p(TPD2T-CPDT) upon electro-oxidation (at +2.2, +2.2, +2.0 V, +2.0, +1.5, and +1.6 V) are shown in Fig. 3h. Overall, all seven polymers exhibit grey colours of different hues in the oxidised state.

3.5. Colorimetric analysis

Colorimetric analysis was performed to quantify the colours of the polymers in the neutral and oxidised states, using the CIE 1976 L^* a^* b^* colour space, where L^* defines the lightness of the colour from a scale of 0 (brightest white) to 100 (darkest black), a^* defines the extent of redness (positive) against greenness (negative) of the colour, and b^*, the extent of yellowness (positive) against blueness (negative) of the colour. The corresponding colour coordinates are shown in Fig. S5 (SI), while Fig. S6 (SI) illustrates the data using a 2-dimensional a^* *vs.* b^* plot, as well as a 1-dimensional L^* scale.

In the neutral state, a general decrease in L^* is observed from p(TPD2T-T) to p(TPD2T-2T), p(TPD2T-TT) and p(TPD2T-3T), indicating progressively darker colours with increasing conjugation length of the oligothiophene donors. The introduction of stronger EDOT, DTP and CPDT donors, led to more drastic reduction in L^* for p(TPD2T-EDOT), p(TPD2T-DTP), and p(TPD2T-CPDT) with respectively. Upon electro-oxidation, all polymers show an increase in L^*, corresponding to lighter colour and greater transmissivity. The magnitude of this change (ΔL^*) generally increases with donor strength, with p(TPD2T-DTP) exhibiting the largest ΔL^* (+10.43), while p(TPD2T-T) shows only a minimal change (+0.53). It is noted that absolute L^* values may also be influenced by variations in film thickness (Table S2), although not significantly. For example, p(TPD2T-CPDT) has a thinnest film of 59.2 nm thickness but also the darkest neutral colour (L^* = 76.67), whereas p(TPD2T-TT) has the thickest film of 226.8 nm thickness, but the third lightest neutral colour (L^* = 86.19).

Analysis of the a^* coordinate reveals that most polymers exhibit positive values in the neutral state, indicating a red component that increases from p(TPD2T-T) to p(TPD2T-TT), in line with increasing effective conjugation in the donor. However, incorporation of stronger donors leads to a reduction in a^* that appears to correlate with donor strength (CPDT < EDOT < DTP), with p(TPD2T-DTP) displaying negative values, indicative of a shift towards greenish-blue hues. A clearer trend is observed in the b^* coordinate. While polymers with weaker donors (T, 2T, TT) show small positive or near-zero b^* values (slightly yellowish), increasing conjugation (3T, CPDT), and especially stronger donors (CPDT, EDOT, DTP) result in increasingly negative b^* values, corresponding to more pronounced blue colouration. This is consistent with the red-shifted absorption profiles observed for these systems.

In the oxidised state, the colour coordinates converge towards "true black" (a^* = 0, b^* = 0) (Fig. S6, SI), giving rise to greyish hues across all seven polymers. Compared to the neutral state, polymers with weaker donors show smaller magnitude decreases in b^* (become bluer) upon oxidation, whereas those with stronger donors (EDOT, DTP, CPDT) exhibit larger magnitude increases in b^* (become yellower), with p(TPD2T-DTP) displaying the largest change (Δb^* = +12.39). Meanwhile, increasing the extent of donor's conjugation from T to 2T, TT, and 3T increases the magnitude of change in a^* as oxidised polymers become less red (Δb^* = −1.72, −4.46, −8.61, and −10.56, respectively). Polymers with stronger donors appear to have smaller Δb^* with p(TPD2T-DTP) having a Δb^* of +0.28 instead.

3.6. Chronoamperometry and EC kinetic switching studies

Chronoamperometry studies were conducted to further evaluate the EC switching behaviour of the seven polymers, where transmittance at the respective visible and NIR wavelengths was monitored under alternating positive and negative potentials of ±2.2 V for p(TPD2T-T) and ±2.0 V for the rest, applied at switching intervals (Δt) of 40, 30, 20, 10, and 5 s over several cycles (Fig. 4). p(TPD2T-EDOT) and p(TPD2T-DTP) exhibit the highest OCs of 23.8 and 20.0% for visible switching (at 595 and 608 nm), and 46.7 and 44.8% for NIR switching (at 1800 and 1400 nm), respectively. The polymers' OCs decrease with decreasing Δt, reflecting incomplete switching at shorter time intervals. This effect is particularly pronounced for p(TPD2T-T), p(TPD2T-2T), and p(TPD2T-CPDT), where their NIR OCs decrease from 27.4, 20.2, and 23.7% at Δt = 40 s to 11.7, 12.9, and 9.8% at Δt = 5 s, respectively, while the corresponding visible OCs decrease from 20.0, 12.4, and 18.2% to 10.6, 6.9, and 7.7%, respectively. In contrast, p(TPD2T-3T), p(TPD2T-EDOT), and p(TPD2T-DTP) show smaller reductions in OCs, with NIR contrasts decreasing from 42.1, 46.8, and 44.8% at Δt = 40 s to 31.8, 36.8, and 36.6% at Δt = 5 s, and visible contrasts from 17.5, 23.8, and 20.0% at Δt = 40 s to 11.3, 20.2, and 18.5% Δt = 5 s, respectively.

The above trends are closely related to the polymers' switching τ_s (Table S2, SI), where τ_{ox} and τ_{re} denote the times required for electro-oxidation and recovery, respectively. All seven polymers exhibit shorter τ_{re} than τ_{ox} at both visible and NIR wavelengths while switching at NIR wavelengths is generally slightly slower than at visible wavelengths. Polymers incorporating stronger donors show faster switching. (TPD2T-EDOT) and p(TPE2T-DTP) exhibit relatively shorter τ_{ox}/τ_{re} of 9.0/1.7 s and 4.3/0.7 s, respectively, for visible EC switching, and 11.9/1.3 and 6.8/1.2 s, respectively, for NIR EC switching. The faster switching of these polymers enable more complete EC transitions within shorter Δt, thereby allowing them to retain higher OCs under rapid switching conditions.

The colouration efficiency (CE) of the seven polymers was measured. Amongst them, p(TPD2T-EDOT) and p(TPD2T-DTP) exhibited exceptionally high CEs of 720.7 and 801.1 cm^2 cm^{-1} for EC switching at 595 and 608 nm, respectively, and excellent CEs of 1012.1 and 1358.5 cm^2 cm^{-1} for that in 1800 and 1400 nm, respectively. Comparatively, the other polymers show relatively lower CEs of 207 to 377 cm^2 cm^{-1} for visible EC switching, and 200 to 630 cm^2 cm^{-1} for NIR EC switching.

Open-circuit memory retention was evaluated at both visible and NIR wavelengths to assess the ability of the polymers to maintain their coloured (charged) states after removal of the applied potential. The transmittance of fully oxidised electrochromic devices (ECDs) was monitored over 10 min under

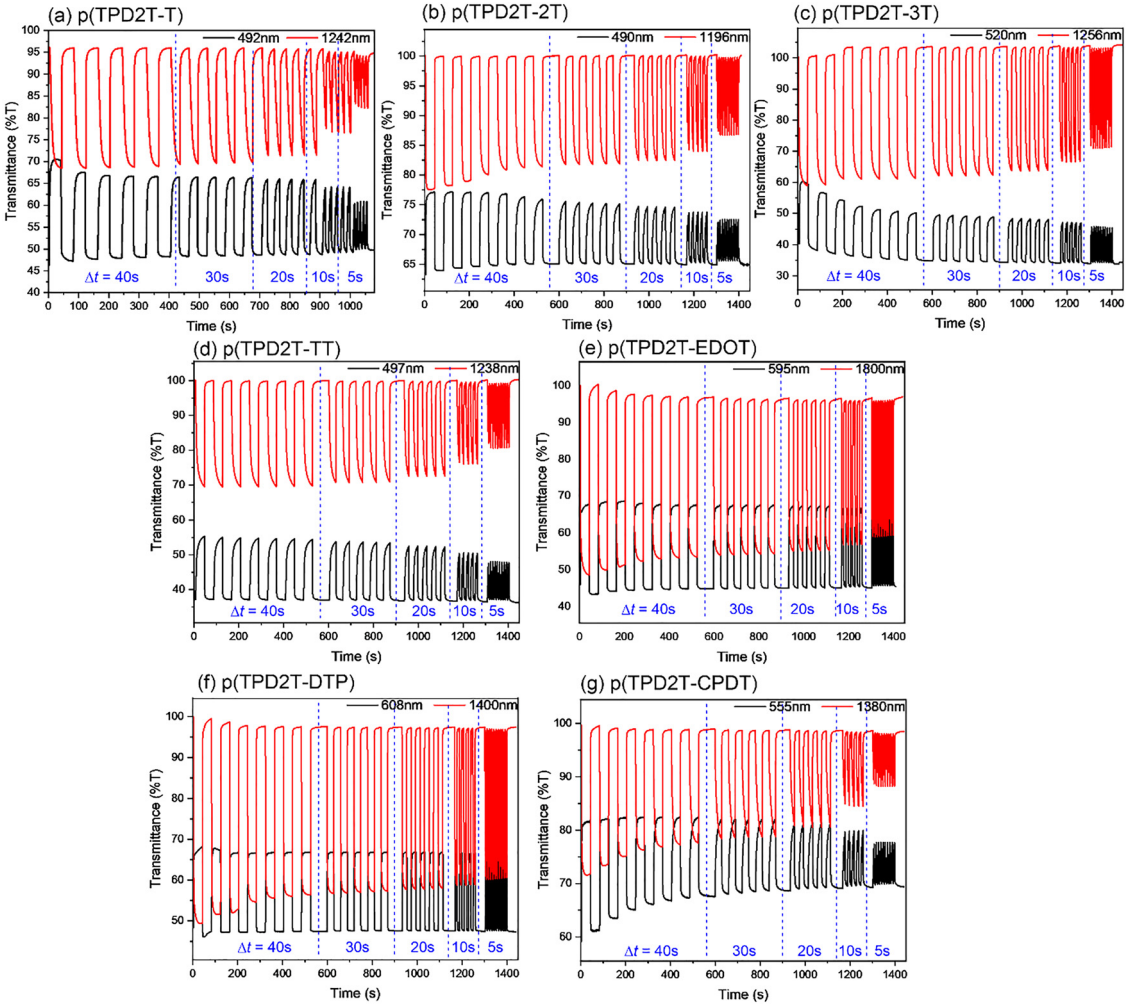

Fig. 4 Chronoabsorptometry studies on the transmittance changes (%*T*) to the visible and NIR wavelengths of study for the polymers (a) p(TPD2T-T), (b) p(TPD2T-2T), (c) p(TPD2T-3T), (d) p(TPD2T-TT), (e) p(TPD2T-EDOT), (f) p(TPD2T-DTP), and (g) p(TPD2T-CPDT) performed at ±2.2, ±2.0, ±2.0, ±2.0, ±2.0, ±2.0, and ±2.0 V, respectively, at different interval times (Δ*t*) of 40, 30, 20, 10, and 5 s.

open-circuit conditions. All polymers exhibit some degree of transmittance decay, indicating partial loss of the charged state over time (Fig. S7, SI). However, the extent of retention correlates strongly with donor strength. p(TPD2T-DTP) shows the best memory performance, retaining 75.4% and 73.2% of its initial transmittance at visible and NIR wavelengths, respectively, after 10 min. This is followed by p(TPD2T-EDOT), which retains 67.9% (visible) and 49.6% (NIR). In contrast, polymers bearing weaker donors, such as p(TPD2T-T) and p(TPD2T-TT), exhibit significantly poorer retention, maintaining only 19.7% and 16.5% (visible) and 19.2% and 22.1% (NIR), respectively.

The EC switching performance of the seven polymers reveals a clear structure–property relationship governed primarily by donor strength. The superior performance of p(TPD2T-EDOT) and p(TPD2T-DTP) in terms of OC, τ, CE, and open-circuit memory retention can be attributed to the strong electron-donating characteristic of EDOT and DTP, which enhances donor–acceptor interactions, lowers the bandgaps and oxidation potentials, and facilitates more efficient charge injection and extraction. This also promotes greater π-electron delocalisation along the polymer backbone, thereby stabilising oxidised polaronic and bipolaronic states. As a result, these polymers exhibit larger optical modulation, faster switching kinetics, higher optical modulation per injected charge,[65–67] and slower charge recombination under open-circuit conditions. In contrast, secondary factors such as conjugation length (T to 3T) and structural rigidity (TT and CPDT) mainly influence optical absorption and colour tuning through bandgap modulation and improved backbone planarity, but exert a less pronounced effect on switching kinetics within this polymer series. We also acknowledge that the relatively smoother film morphologies of p(TPD2T-EDOT) and p(TPD2T-DTP) might have also contributed to these stellar performances (Fig. S4, SI). Meanwhile, the polymer's M_w does not appear to have any influence.

The long-term EC switching stability of the p(TPD2T-3T), p(TPD2T-EDOT) and p(TPD2T-DTP) polymers at their respective NIR wavelengths of study was further assessed by monitoring the transmittance at 1256, 1800, and 1400 nm, respectively, over 3000 cycles while switching at ±1.8 V, at a Δ*t* of 20 s (Fig. S8, SI). Both polymers p(TPD2T-3T) and p(TPD2T-EDOT)

exhibited relatively gradual changes in OCs indicating good durability. They experienced 10.7 and 15.1% loss to their initial OCs after 1000 cycles, respectively, which increased to 20.9 and 24.8% loss, respectively, after 3000 cycles. The relatively high molecular weight of p(TPD2T-3T) could have contributed to its robust cycling stability by creating physical entanglements that provide exceptional mechanical resilience and long-term cycling stability,[68] whilst the electron-rich EDOT units in p(TPD2T-EDOT) significantly lower the operating oxidation potential and stabilize oxidized states through resonance delocalization and a more favourable oxidation profile.[69] On the other hand, p(TPD2T-DTP) showed a more pronounced decrease in OC, losing 35.6% of its initial OC after 1000 cycles, and retaining 51.5% of the initial OC after 3000 cycles. This poorer stability may reflect the greater susceptibility of p(TPD2T-DTP) to over-oxidation, consistent with it having the highest HOMO level and lowest oxidation onset potential among the seven polymers (Table 1).

3.7. Electrofluorochromic (EFC) studies

Electrofluorochromism is the modulation of a material's fluorescence, commonly the intensity, through external applied voltages.[70–72] In addition to EC properties, we also studied the EFC properties of polymers p(TPD2T-T), p(TPD2T-2T), p(TPD2T-3T), p(TPD2T-TT), and p(TPD2T-CPDT) which exhibit red/far-red fluorescence in the solid thin film state. As shown in Fig. 5, incrementally increasing the applied positive voltages led to a decrease in fluorescence intensities and eventual fluorescence quenching of all five polymers. The onset of the decrease in fluorescence intensity started at between *ca.* +0.6 and +0.9 V for p(TPD2T-T), p(TPD2T-2T) and p(TPD2T-3T) but much earlier at *ca.* +0.2 V for p(TPD2T-TT), and p(TPD2T-CPDT). The ECD fluorescence of the five polymers were totally quenched at +1.6, +1.4, +1.3, +1.2, and +1.4 V, respectively. Chronofluorometry EFC switching studies for p(TPD2T-T), p(TPD2T-2T), p(TPD2T-3T), p(TPD2T-TT) were performed at their respective λ_{PL} of 710, 708, 697, and 710 nm, by alternating voltages of ±1.8, ±1.6, ±1.6, and ±2.2 V, respectively, at different Δts of 40, 30, 20, 10, and 5 s for a few cycles (Fig. S9, SI). The fluorescence signals were generally stable and reversible for all four polymers across the different switching Δts, with the exception of p(TPD2T-3T) which shows a slight decrease in fluorescence intensity contrasts at a Δt of 40 s. Switching at a Δt of 40 s, the four polymers were able to achieve contrasts ($I_{OFF/ON}$, determined by the ratio of the maximum and minimum fluorescence intensities between application of positive and negative voltages) of *ca.* 11.7, 3.6, 8.7, and 3.0, respectively. Meanwhile, the EFC switching signals of p(TPD2T-CPDT) appear less reproducible and more unstable over the different Δts, with a much lower $I_{OFF/ON}$ of *ca.* 1.3 at Δt = 40 s (Fig. S9, SI).

3.8. Comparison with reported TPD-based EC polymers

Table S3 (SI) summarises the key parameters of TPD-based conjugated polymers reported for EC applications. Onal *et al.* electropolymerized three polyhedral oligomeric silsesquioxane-functionalized TPD monomers with two adjacent thiophene, EDOT, and 3,4-propylenedioxythiophene (ProDOT) donors, respectively, and performed oxidative chemical polymerization for the latter two monomers bearing EDOT and ProDOT donors.[53] The polymers reveal a range of neutral colours of pink, blue, and purple, transiting to grey, light blue and transparent upon electro-oxidation. Song *et al.* prepared an alternating polymer with a TPD acceptor and ProDOT donor *via* Stille coupling polymerization

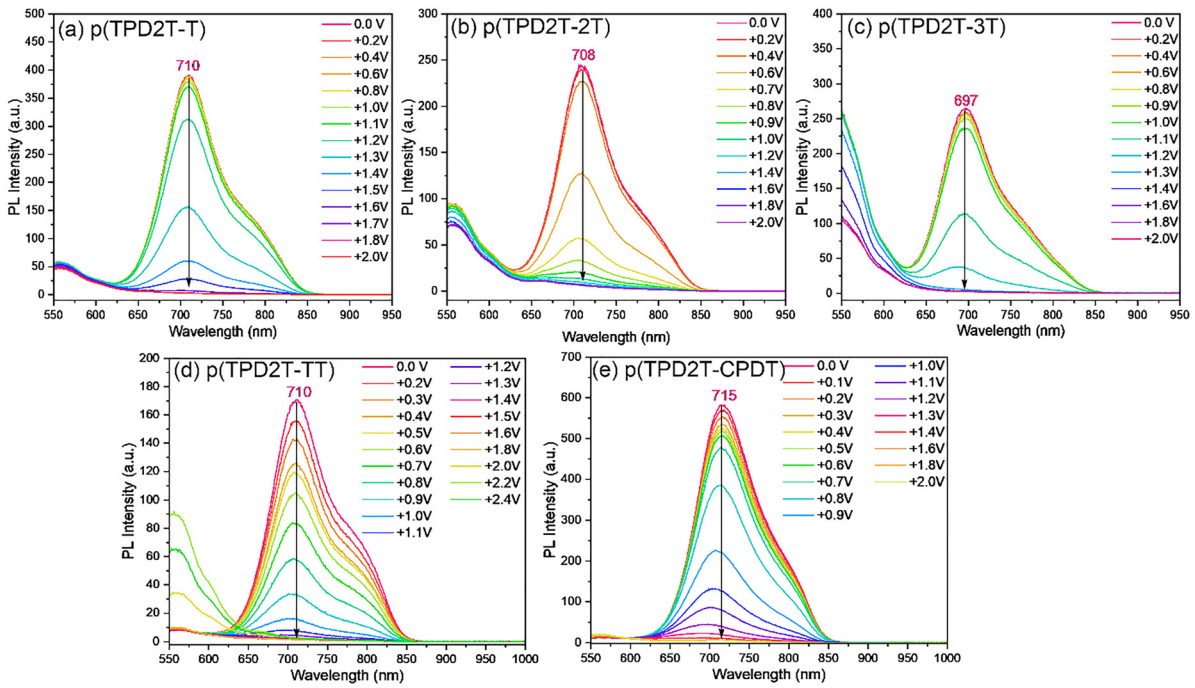

Fig. 5 EFC spectroelectrochemistry studies of polymers (a) p(TPD2T-T), (b) p(TPD2T-2T), (c) p(TPD2T-3T), (d) p(TPD2T-TT), and (e) p(TPD2T-CPDT).

which shows purple-to-transparent grey EC switching in a liquid-based sandwich device.[54] Zhen *et al.* electropolymerized a ProDOT-TPD-ProDOT monomer which switches with an OC of 27.1% in the NIR region (at 1000 nm) with applied positive voltages.[55] Unfortunately, other EC properties are unavailable in the study.

Structurally, this work expands the scope of donors for TPD-based EC polymers compared to existing work, with the inclusion of other thiophene-based donors such as TT, DTP, and CPDT. As shown in Table S3 (SI), all seven polymers show comparable E_g to those reported by Onal *et al.* and Song *et al.* Through the use of four and five thiophenes, as well as TT donors, we are also able to achieve brown neutral colouration not reported in prior work. Meanwhile, the greyish colourations of our TPD polymers in the charged state are consistent with those of previously reported work. The OCs obtained for our polymers were in the range of 17.5–23.8% for EC switching in the visible wavelength region, and 20.2–46.4% for EC switching in the NIR wavelength region, which are comparable to prior art (18–52%). Meanwhile, the τ_{ox} of our polymers are slightly longer than those reported while the CEs of our polymers are comparable to those reported, although those of p(TPD2T-EDOT) and p(TPD2T-DTP) (1012.1 and 1358.5 $cm^2\ C^{-1}$, respectively) were the highest recorded for TPD-based EC polymers thus far.

For long-term switching stability, our work has demonstrated that p(TPD2T-3T) and p(TPD2T-EDOT) can exhibit considerable stability up to 3000 cycles with 20.9 and 24.8% loss in initial OCs. This is significantly higher than the 200 cycles with 20% drop in OC reported by Song *et al.* While these results may be considered comparable to some other simple D–A type polymers, such as benzimidazole-EDOT[73] and isoindigo-EDOT[32]-based polymers retaining 76 and 92% of electroactivity after 4000 switching cycles, respectively, they are still modest compared to some recently reported multi-donor D–A type conjugated polymers, such as the quinacridone-CPDT-ProDOT copolymer reported by Li *et al.*,[74] and a black-to-transmissive BTD-fluorene-ProDOT copolymer reported by Chen *et al.*[75] which retained 88.4 and 99% of their initial OCs after 100 000 and 126 000 cycles, respectively.

Finally, thin film ECD λ_{PL} values of the five polymers studied herein (697–715 nm) are more red-shifted than that of the TPD-ProDOT polymer reported by Song *et al.* (672 nm), with the $I_{OFF/ON}$ contrast for p(TPD2T-3T) of 11.7 comparable to that of the reported polymer ($I_{OFF/ON}$ 12.9).[54]

However, it is worth noting that the ECD structures differ between our work and that of prior arts, as our work fabricated sandwich type full-cell thin film devices with a polymer gel electrolyte, whilst Onal *et al.* and Zhen *et al.* adopted hall-cell ECDs, and Song *et al.*, a "liquid-based" full cell device. Hence, EC and EFC switching parameters such as OCs and response times may not be directly comparable across the different studies.

4. Conclusion

In summary, seven TPD-based polymers incorporating thiophene-based donors of varying conjugation length, donor strength, and structural rigidity were synthesised and systematically investigated. The polymers exhibit tuneable neutral colours ranging from light grey to brown, blue, and purple, which transition to lighter hues of grey upon electro-oxidation. Colorimetric analysis indicates that stronger electron-donating units, such as EDOT and DTP, produce darker neutral colours with reduced redness and enhanced blueness, consistent with increased ICT. Further EC studies reveal donor strength as the dominant factor influencing EC switching performance, with p(TPD2T-EDOT and p(TPD2T-DTP) exhibiting higher OCs, shorter τs, higher CEs, and better open-circuit memory retention than the other polymers. In comparison, donors' effective conjugation length and structural rigidity play secondary roles, primarily influencing optical absorption and colour tuning. Meanwhile, the stellar long-term switching stability of p(TPD2T-3T) reflects the influence of its (exceptionally high) M_w in EC cycling durability. Given the promising performance of these polymers, future work may entail further device optimization and integration into practical applications and real world technologies. Additional EFC studies of polymers exhibiting thin film fluorescence showed quenching of red/far-red fluorescence (λ_{PL} 697 to 715 nm) with p(TPD2T-T) having the largest contrasts of $I_{OFF/ON}$ of 11.7. Given the current scarcity of and growing interest in far-red/NIR emitters for EFC applications,[76,77] TPD could also serve as a promising building block for future NIR-EFC polymeric materials.

Overall, this work demonstrates the effective tuning of colours and EC properties of TPD-based conjugated polymers through systematic donor engineering. The findings provide important structure–property insights, well addressing the current scarcity of comprehensive studies on TPD-based EC systems. These critical findings will be useful to guide the development of high performance EC and EFC materials with tuneable switching characteristics tailored to the functional needs of different end applications, such as smart windows for energy-saving, user-comfort and aesthetics in green buildings and automobiles. Furthermore, given the broad applicability of TPD-based conjugated polymers in other applications such as photovoltaics, field effect transistors, and thermoelectrics, as reported, this work may guide the development of multi-functional TPD-based EC conjugated polymers for advanced uses in a sustainable urban environment for greater energy-efficiency.[78] With different combinations of donor and acceptor building blocks explored thus far in the development of EC and EFC conjugated polymers, there will also be opportunities to leverage on artificial intelligence and machine learning in future EC polymer materials design.

Author contributions

K. C. Chong contributed to methodology and investigation – polymer synthesis and characterization, device fabrication and testing, visualization, and writing the original draft of the manuscript. K. L. O. Chin and R. Tao supported investigations through the characterization of polymers, device fabrication, and testing. S. J. Ang provided computational studies support

(methodology and investigation). J. Xu provided supervision, funding acquisition, and review and editing of the manuscript. M. H. Chua conceptualized this work and provided supervision, project administration, and funding acquisition. He was also involved in the visualization and writing (review and editing) of the manuscript.

Conflicts of interest

The authors have no conflicts to declare.

Data availability

The data supporting this article have been included as part of the supplementary information (SI). Supplementary information: Scheme S1, Fig. S1–S9, Tables S1–S3, NMR and FTIR spectra, GPC chromatograms, and other experimental details and computational data. See DOI: https://doi.org/10.1039/d6tc00224b.

Acknowledgements

The authors would like to acknowledge funding support from the Agency for Science, Technology and Research, Singapore (A*STAR) HTCO Fund (grant number: C231218001). The computational calculation work was supported by the A*STAR Computational Resource Centre through the use of its high performance computing facilities. The authors would also like to thank Ms Ping Luo for the support in the SEM studies.

References

1 T. Ahmed, A. Mazumder, S. Kuriakose, A. Dubey, A. Elbourne, J. Ren, V. Krishnamurthi, E. Kandare, I. H. Abidi, E. Della Gaspera, S. Balendhran and S. Walia, *Nanoscale*, 2025, **17**, 18049–18076.
2 H. Fu, L. Zhang, Y. Dong, C. Zhang and W. Li, *Mater. Chem. Front.*, 2023, **7**, 2337–2358.
3 H. Fan, W. Wei, C. Hou, Q. Zhang, Y. Li, K. Li and H. Wang, *J. Mater. Chem. C*, 2023, **11**, 7183–7210.
4 M. H. Chua, T. Tang, K. H. Ong, W. T. Neo and J. W. Xu, in *Electrochromic Smart Materials: Fabrication and Applications*, ed. J. W. Xu, M. H. Chua and K. W. Shah, The Royal Society of Chemistry, 2019, ch. 1, pp. 1–21.
5 R. J. Mortimer, A. L. Dyer and J. R. Reynolds, *Displays*, 2006, **27**, 2–18.
6 T. Abidin, Q. Zhang, K.-L. Wang and D.-J. Liaw, *Polymer*, 2014, **55**, 5293–5304.
7 B. Bezgin Carbas, E. G. Cansu Ergun and S. Ozdemir Hacioglu, *Chem. Eng. J.*, 2025, **526**, 169629.
8 B. Bezgin Carbas, *Polymer*, 2022, **254**, 125040.
9 B. Bezgin Carbas, *ACS Appl. Polym. Mater.*, 2025, **7**, 4051–4076.
10 B. B. Carbas, S. Özbakır and Y. Kaya, *Synth. Met.*, 2023, **293**, 117298.
11 E. G. Cansu Ergun and B. Bezgin Carbas, *Mater. Today Commun.*, 2022, **32**, 103888.
12 B. Bezgin Carbas and E. G. C. Ergun, *Eur. Polym. J.*, 2022, **175**, 111363.
13 M. H. Chua, Q. Zhu, T. Tang, K. W. Shah and J. Xu, *Sol. Energy Mater. Sol. Cells*, 2019, **197**, 32–75.
14 A. L. Dyer, E. J. Thompson and J. R. Reynolds, *ACS Appl. Mater. Interfaces*, 2011, **3**, 1787–1795.
15 C. M. Amb, A. L. Dyer and J. R. Reynolds, *Chem. Mater.*, 2011, **23**, 397–415.
16 W. T. Neo, Q. Ye, S.-J. Chua and J. Xu, *J. Mater. Chem. C*, 2016, **4**, 7364–7376.
17 R. Rybakiewicz-Sekita, P. Toman, R. Ganczarczyk, J. Drapala, P. Ledwon, M. Banasiewicz, L. Skorka, A. Matyjasiak, M. Zagorska and A. Pron, *J. Phys. Chem. B*, 2022, **126**, 4089–4105.
18 S. Yan, L. Zhang, X. Lv, J. Sun, Y. Zhang and C. Zhang, *Adv. Photon. Res.*, 2022, **3**, 2000199.
19 P. M. Beaujuge and J. R. Reynolds, *Chem. Rev.*, 2010, **110**, 268–320.
20 Q. Yang, A. Vriza, C. A. Castro Rubio, H. Chan, Y. Wu and J. Xu, *Chem. Mater.*, 2024, **36**, 2602–2622.
21 B. Liu, Y. Yan and M. Liu, *Nanoscale*, 2025, **17**, 7865–7876.
22 A. Pron and M. Leclerc, *Prog. Polym. Sci.*, 2013, **38**, 1815–1831.
23 B. Li and Y. Lv, *Adv. Opt. Mater.*, 2025, **13**, e01835.
24 Y. Zhou, W. Zhang and G. Yu, *Chem. Sci.*, 2021, **12**, 6844–6878.
25 X. Guo, A. Facchetti and T. J. Marks, *Chem. Rev.*, 2014, **114**, 8943–9021.
26 D. Giri, S. K. Saha, I. Anderson, A. Chakraborty, J. Kala, J. S. Müller, J. Nelson, R. K. Canjeevaram Balasubramanyam and S. Patil, *Adv. Funct. Mater.*, 2025, **35**, 2410815.
27 B. Lim, S.-Y. Han and Y.-C. Nah, *Org. Electron.*, 2018, **63**, 23–28.
28 X. Liu, L. Kong, H. Du, Y. Zhang, J. Zhao and Y. Xie, *Org. Electron.*, 2019, **64**, 223–235.
29 J. Z. Low, W. T. Neo, Q. Ye, W. J. Ong, I. H. K. Wong, T. T. Lin and J. Xu, *J. Polym. Sci., Part A: Polym. Chem.*, 2015, **53**, 1287–1295.
30 M. H. Chua, S. H. G. Toh, P. J. Ong, Z. M. Png, Q. Zhu, S. Xiong and J. Xu, *Polym. Chem.*, 2022, **13**, 967–981.
31 X. Cheng, Y. Ma, X. Ju, W. Zhao, J. Zhao, Q. Li, Z. Sang, H. Du and Y. Zhang, *Synth. Met.*, 2020, **270**, 116589.
32 H. Gu, S. Ming, K. Lin, S. Chen, X. Liu, B. Lu and J. Xu, *Electrochim. Acta*, 2018, **260**, 772–782.
33 H. Gu, K. Wang, Z. Wu, N. Jian, H. Ma, Q. Zhao, Y. Deng, J. Liu, J. Xu, X. Wang, Y. Yu and B. Lu, *Electrochim. Acta*, 2021, **399**, 139418.
34 H. Miao, H. Zhang, L. Li and X. He, *Adv. Opt. Mater.*, 2025, **13**, 01212.
35 I. E. Park, A. Hoff, C. Beaumont, B. S. Gelfand, R. D. Pettipas and G. C. Welch, *J. Mater. Chem. C*, 2024, **12**, 1710–1717.
36 J. Hou, S. Zhang, T. L. Chen and Y. Yang, *Chem. Commun.*, 2008, 6034–6036.
37 B. He, W. T. Neo, T. L. Chen, L. M. Klivansky, H. Wang, T. Tan, S. J. Teat, J. Xu and Y. Liu, *ACS Sustain. Chem. Eng.*, 2016, **4**, 2797–2805.

38 B. Y. K. Hui, K. L. O. Chin, J. J. L. Lim, X. Y. D. Soo, X. Lu, Q. Zhu, X. Liu, J. Xu and M. H. Chua, *Chem. – Asian J.*, 2024, **19**, e202400236.
39 Q. Ye, W. T. Neo, C. M. Cho, S. W. Yang, T. Lin, H. Zhou, H. Yan, X. Lu, C. Chi and J. Xu, *Org. Lett.*, 2014, **16**, 6386–6389.
40 Q. Ye, W. T. Neo, T. Lin, J. Song, H. Yan, H. Zhou, K. W. Shah, S. J. Chua and J. Xu, *Polym. Chem.*, 2015, **6**, 1487–1494.
41 C. M. Cho, Q. Ye, W. T. Neo, T. Lin, X. Lu and J. Xu, *Polym. Chem.*, 2015, **6**, 7570–7579.
42 T. P. Vo, M. H. Chua, S. J. Ang, K. L. O. Chin, X. Y. D. Soo, Z. M. Png, T. L. D. Tam, Q. Zhu, D. J. Procter and J. Xu, *Polym. Chem.*, 2022, **13**, 6512–6524.
43 P. He, X.-L. Qiao, Q. Qian and H.-X. Li, *Chin. Chem. Lett.*, 2016, **27**, 1277–1282.
44 C. Zhao, F. Yang, D. Xia, Z. Zhang, Y. Zhang, N. Yan, S. You and W. Li, *Chem. Commun.*, 2020, **56**, 10394–10408.
45 S. Beaupré, A. Pron, S. H. Drouin, A. Najari, L. G. Mercier, A. Robitaille and M. Leclerc, *Macromolecules*, 2012, **45**, 6906–6914.
46 Y. Wang, J. Xiang and X. Gao, *Chin. Sci. Bull.*, 2024, **69**, 45–57.
47 Q. Wu, M. Wang, X. Qiao, Y. Xiong, Y. Huang, X. Gao and H. Li, *Macromolecules*, 2013, **46**, 3887–3894.
48 K. H. Park, J.-Y. Go, B. Lim and Y.-Y. Noh, *J. Polym. Sci.*, 2022, **60**, 429–485.
49 X. Guo, R. P. Ortiz, Y. Zheng, M.-G. Kim, S. Zhang, Y. Hu, G. Lu, A. Facchetti and T. J. Marks, *J. Am. Chem. Soc.*, 2011, **133**, 13685–13697.
50 X. Fan, S. Deng, X. Cao, B. Meng, J. Hu and J. Liu, *ACS Appl. Mater. Interfaces*, 2024, **16**, 46741–46749.
51 X. Zhang, M. Chang, D. Wang, L. Wang, X. Yang, Z. Ben, Q. Zhang and Y. Lu, *J. Colloid Interface Sci.*, 2025, **682**, 1151–1163.
52 M. Chang, X. Zhang, L. Wang, D. Wang, Q. Zhang and Y. Lu, *Green Chem.*, 2024, **26**, 466–476.
53 D. Çakal, A. Cihaner and A. M. Önal, *Electrochim. Acta*, 2021, **377**, 138064.
54 P. Wu, S. Zhang, W. Zhang and W. Song, *Dyes Pigm.*, 2023, **219**, 111566.
55 Z. Xu, S. Ming, T. Zhang, M. Li and S. Zhen, *Luminescence*, 2024, **39**, e4843.
56 X. Zhang, T. T. Steckler, R. R. Dasari, S. Ohira, W. J. Potscavage, S. P. Tiwari, S. Coppée, S. Ellinger, S. Barlow, J.-L. Brédas, B. Kippelen, J. R. Reynolds and S. R. Marder, *J. Mater. Chem.*, 2010, **20**, 123–134.
57 S. Hayashi, *Mater. Adv.*, 2020, **1**, 632–638.
58 B. de Souza, *Angew. Chem., Int. Ed.*, 2025, **64**, e202500393.
59 C. Bannwarth, S. Ehlert and S. Grimme, *J. Chem. Theory Comput.*, 2019, **15**, 1652–1671.
60 S. Ehlert, M. Stahn, S. Spicher and S. Grimme, *J. Chem. Theory Comput.*, 2021, **17**, 4250–4261.
61 H. S. Yu, X. He, S. L. Li and D. G. Truhlar, *Chem. Sci.*, 2016, **7**, 5032–5051.
62 A. V. Marenich, C. J. Cramer and D. G. Truhlar, *J. Phys. Chem. B*, 2009, **113**, 6378–6396.
63 J.-L. Brédas, D. Beljonne, V. Coropceanu and J. Cornil, *Chem. Rev.*, 2004, **104**, 4971–5004.
64 F. Neese, *WIREs Comput. Mol. Sci.*, 2025, **15**, e70019.
65 K. Lin, C. Wu, S. Ming, D. Xie, J. Lin, Z. Huo, F. Lu, C. Feng, H. Liu, H. Liu, J. Li and Y. Wang, *Dyes Pigm.*, 2025, **232**, 112504.
66 K. Lin, C. Wu, G. Zhang, Z. Wu, S. Tang, Y. Lin, X. Li, Y. Jiang, H. Lin, Y. Wang, S. Ming and B. Lu, *Molecules*, 2022, **27**, 8424.
67 C. Wu, H. Chen, J. Tan, D. Zhou, H. Liang, S. Zhen, H. Liu, Y. Wang and K. Lin, *Sol. Energy Mater. Sol. Cells*, 2023, **257**, 112355.
68 S. Hayashi, S.-i Yamamoto and T. Koizumi, *Sci. Rep.*, 2017, **7**, 1078.
69 J. Roncali, P. Blanchard and P. Frère, *J. Mater. Chem.*, 2005, **15**, 1589–1610.
70 M. H. Chua, Q. Zhu, K. W. Shah and J. Xu, *Polymers*, 2019, **11**, 98.
71 K. Nakamura, K. Kanazawa and N. Kobayashi, *J. Photochem. Photobiol., C*, 2022, **50**, 100486.
72 G. A. Corrente and A. Beneduci, *Adv. Opt. Mater.*, 2020, **8**, 2000887.
73 S. Al-Ogaidi, B. Karabay, L. C. Karabay and A. Cihaner, *J. Electroanal. Chem.*, 2016, **768**, 1–10.
74 J. Li, L. Zhang, J. Cui, X. Lv, M. Feng, M. Ouyang, Z. Chen, D. S. Wright and C. Zhang, *Small*, 2023, **19**, 2303359.
75 D. Chen, Z. Tong, Q. Rao, X. Liu, H. Meng and W. Huang, *Nat. Commun.*, 2024, **15**, 8457.
76 I. Seddiki, B. I. N'Diaye and W. G. Skene, *Molecules*, 2023, **28**, 3225.
77 B. Y. K. Hui, R. Tao, K. L. O. Chin, X. Y. D. Soo, A. Sng, S. A. A. Abedi, K. C. Chong, X. Liu, J. Xu and M. H. Chua, *Adv. Opt. Mater.*, 2026, **14**, e02075.
78 D. Chen, M. H. Chua, Q. He, Q. Zhu, X. Wang, H. Meng, J. Xu and W. Huang, *Chem. Eng. J.*, 2025, **503**, 157820.